An interpretation of high spectral resolution remote sensing reflectance

Zhongping Lee[1], Kendall L. Carder[1], Steve K. Hawes[1], Robert G. Steward[1], Thomas G. Peacock[1] and Curtiss O. Davis[2]

1 Department of Marine Science
University of South Florida
140 Seventh Avenue South, FL 33701
Tel. (813)893-9503

2 Jet Propulsion Laboratory, California Institute of Technology
4800 Oak Grove Blvd., Pasadena, CA 91109

ABSTRACT

Remote sensing reflectance is easier to interpret for the open ocean than for coastal regions since bottom reflectance and fluorescence from colored dissolved organic matter (CDOM) need not be considered. For estuarine or coastal waters, the reflectance is less easy to interpret because of the variable terrigenous CDOM, suspended sediments, and bottom reflectance, since these factors do not covary with the pigment concentration. To estimate the pigment concentration, the water-leaving radiance signal must be corrected for the effects of these non-covarying factors. A two-parameter model is presented to model remote sensing reflectance of the water-column, to which contributions due to CDOM fluorescence, water Raman scattering and bottom reflectance have been added. The purpose of this research is to try to understand the separate contributions of the water-column, CDOM fluorescence, water Raman and bottom reflectance for stations on the West Florida Shelf and Lake Tahoe. This model requires data with spectral resolution of 10 nm or better, consistent with that provided by AVIRIS and expected from HIRIS.

1. INTRODUCTION

The use of the power-law of spectral radiance ratios[1,2] to measure pigment concentrations requires that the water leaving radiance is largely determined by variations in the pigment concentration with all other optical constituents covarying along with this quantity. The method works quite well for the open ocean or "Case I" waters[3]. This is because the water-leaving radiance of open ocean waters is not affected by bottom reflectance, land run-off, and suspended sediments. Although aeolian dust may be carried by winds to the open ocean[4], the dominant effect of the particulates may still derive from phytoplankton[5].

The power-law approach can be much less accurate for estuarine and/or coastal areas[6], however, due to the lack of covariance of many of the optical constituents with chlorophyll pigments. In these areas, the water-leaving radiance may include not only parts due to elastic scattering by water molecules, phytoplankton detritus, suspended particulates, bottom reflectance, but may also include the in-elastic scattering of CDOM fluorescence, and water Raman scattering. Thus, changes in ocean color due to

suspended sediments or dissolved organic matter may be interpreted as changes in pigment concentration[6,7]. How the above components influence the power-law is not known very clearly.

It is important to have a good estimate of the pigment concentration for the coastal area since the shelf and slope regions provide over half of the world ocean primary production[8]. For open ocean areas, several good primary production estimates based upon CZCS derived pigment concentration have been obtained[5,7].

For water depth measurements[9,10] or bottom-feature mapping[11], water-leaving radiance or irradiance is usually considered to be due to scattering of water molecules, particulates and the bottom, but not to contributions from the CDOM fluorescence and water Raman. So, the accurate quantification of pigment concentration, water depth, and/or sea grass maps depends on how well we understand all of the contributions to the water-leaving radiance and/or irradiance.

As an initial attemp interpret remote sensing reflectance data including CDOM fluorescence, water Raman effects and .tom reflectance, this work considers the separate contributions of the above components by using high-spectral-resolution data.

2. THEORY

The radiance leaving from ocean water is a complicated mix of signals due to many components. These include the following: absorption by molecules and particulates, elastic scattering by molecules and particulates, and bottom reflectance for shallow waters. Also included are in-elastic scattering due to water, CDOM, chl-a and phycoerythrin molecules. Since chl-a fluorescence occurs in a narrow band and centered around 685nm, it provides an obvious deviation between measured and modeled remote sensing reflectance (R_{rs}) at 685nm if this emission is not considered in the model. Contributions by Gordon[12] and Carder and Steward[13] dealing with chl-a fluorescence have been reported and are not directly considered in this work, due to the small signals found in waters with chl-a less than about 1 mg m^{-1}. It is assumed that the water-leaving radiance is composed of the following four components: elastic scattering from molecules and particles (L_{uw}), bottom reflectance (L_{ub}), Raman scattering (L_{uR}), and CDOM fluorescence (L_{uf}). It is also assumed that there are no cross interactions among these components, so the water-leaving radiance can be expressed as

$$L_u(+,\lambda)=L_{uw}(+,\lambda)+L_{uf}(+,\lambda)+L_{ub}(+,\lambda)+L_{uR}(+,\lambda) \tag{1}$$

The symbols and definitions used in this paper are summarized in Table 1.

The remote sensing reflectance is defined as the ratio of the water-leaving radiance to the downwelling solar irradiance above the water surface,

$$R_{rs}(\lambda)=\frac{L_u(+,\lambda)}{E_d(+,\lambda)} \tag{2}$$

Breaking this equation into contributions from various mechanisms listed in Eq.1, we have

$$R_{rs}(\lambda)=R_{rsw}(\lambda)+R_{rsb}(\lambda)+R_{rsg}(\lambda)+R_{rsR}(\lambda) \tag{3}$$

For a homogeneous and very deep water body, consider a wavelength-independent factor I to describe the influence of the air-sea interface on the remote sensing reflectance. $R_{rsw}(\lambda)$ can be described in terms of values just below the interface as

$$R_{rsw}(\lambda)=I*\frac{L_{rsw}(-,\lambda)}{E_d(-,\lambda)} \tag{4}$$

where, $I=t_+*t_-/n^2$, where t is the transmittance of the air-sea interface, sub + indicates a downward flux, sub - indicates an upward flux, and n is the refractive index of water. For a zenith sun, a nadir-viewing instrument and a calm surface, I=0.533. For larger solar zenith angles and foam-covered seas, t will be lower[14].

The subsurface irradiance reflectance $R_w(-,\lambda)$ is defined as the ratio of the sub-surface upwelling irradiance to the sub-surface downwelling irradiance:

$$R_w(-,\lambda)=\frac{E_{uw}(-,\lambda)}{E_d(-,\lambda)} \tag{5}$$

and Austin[14] has related $E_{uw}(-,\lambda)$ and $L_{uw}(-,\lambda)$ as

$$Q=\frac{E_{uw}(-,\lambda)}{L_{uw}(-,\lambda)} \tag{6}$$

so, $R_{rsw}(\lambda)$ can be expressed as

$$R_{rsw}(\lambda)=\frac{I}{Q}*R_w(-,\lambda) \tag{7}$$

For irradiance reflectance $R_w(-,\lambda)$, Gordon et al[15] obtained a series relation by the Monte Carlo method

$$R_w(-,\lambda)=\sum_{n=0}^{3}\gamma_n\left(\frac{b_b(\lambda)}{a(\lambda)+b_b(\lambda)}\right)^n \tag{8}$$

This equation was simplified[16,17] to

$$R_w(-,\lambda)\doteq.33*\frac{b_b(\lambda)}{a(\lambda)} \tag{9}$$

for $b_b(\lambda)/a(\lambda)$ up to $\sim.25$. The constant 0.33 actually varies slightly with solar zenith angle according to Kirk[18]. The total backscattering coefficient, $b_b(\lambda)$, includes two components: backscattering by molecules $b_{bm}(\lambda)$ and particulate matter $b_{bp}(\lambda)$. The total absorption coefficient $a(\lambda)$ includes contributions due to pure sea water absorption $a_w(\lambda)$, gelbstoff (CDOM) absorption $a_g(\lambda)$ and particulate absorption $a_p(\lambda)$. Inserting these into Eq.9 and suppressing the spectral dependence for convenience, we can write

$R_{rsw}(\lambda)$ as

$$R_{rsw} \doteq \frac{.33I}{a_w + a_g + a_p} * \frac{b_{bm} + b_{bp}}{Q} \tag{10}$$

Eq. 10 is for deep water. When optically shallow water is encountered, the reduced scattering by the water column should be considered; then

$$R_{rsw} = \frac{.33I}{a} * \frac{b_{bm} + b_{bp}}{Q} * [1 - e^{-(K_d + K_u) * H}] \tag{11}$$

for a totally absorbing bottom and water depth H.

If we define the semi-diffuse attenuation coefficient as $\kappa = a + b_b$, then $K_d = D_d\kappa$ and $K_u = D_u\kappa$. D_d and D_u are the distribution functions for the downwelling and upwelling radiance field and are considered depth-independent, and $D_u/D_d \simeq 2$ according to Gordon et al[15]. The remote sensing reflectance from bottom reflectance is defined as $R_{rsb} = L_{ub}(+)/E_d(+)$. Assuming the bottom is Lambertian, with a reflectance $\rho(\lambda)$, then R_{rsb} can be approximated as

$$R_{rsb} \doteq \frac{I}{\pi} \rho * e^{-(K_d + k) * H} \tag{12}$$

where k is the attenuation coefficient for the radiance of a Lambertian source and is approximated as $k \simeq 1.5\kappa$ for vertical radiance[21].

The remote sensing reflectance due to gelbstoff or CDOM fluorescence and water Raman are defined as $R_{rsf} = L_{uf}(+)/E_d(+)$ and $R_{rsR} = L_{uR}(+)/E_d(+)$. In general, these terms are due to in-elastic scattering of CDOM molecules and water molecules indicated by the subscript I. Defining the volume scattering function $\beta_I(\alpha, \lambda_x, \lambda)$ for in-elastic scattering as

$$\beta_I(\alpha, \lambda_x, \lambda) = \frac{T(\alpha, \lambda)}{dV * E(\lambda_x)} \tag{13}$$

where $T(\alpha, \lambda)$ is the intensity of the scattered output radiance, dV is the scattering volume, $E(\lambda_x)$ is the irradiance of the input collimated beam, α is the angle between the input and the output photon directions.

For z positive downward from the surface, θ is the zenith observational angle, and ϕ is the azimuthal observation angle (Fig. 6). With the consideration of isotropic β_I, the in-elastic radiance in the direction θ and the upwelling irradiance at depth z due to the depth interval dz, are

$$dL_f(z,\theta,\lambda)=\int_{\lambda_x}\beta_f(\lambda_x,\lambda)*E_0(z,\lambda_x)*d\lambda_x*\frac{dz}{\cos(\theta)} \tag{14}$$

$$dE_{uf}(z,\lambda)=2\pi\int_{\pi/2}^{\pi}dL_f(z,\theta,\lambda)*\cos(\theta)*\sin(\theta)*d\theta \tag{15}$$

$$=2\pi\int_{\lambda_x}\beta_f(\lambda_x,\lambda)*E_0(z,\lambda_x)*d\lambda_x*dz \tag{16}$$

where $E_0(z,\lambda_x)$ is the scalor irradiance at depth z, and $E_0(z,\lambda_x)=E_{0d}(z,\lambda_x)+E_{0u}(z,\lambda_x)=D_d(1+2R(\lambda_x))E_d(z,\lambda_x)$. Since $E_d(z,\lambda_x)=E_d(0^-,\lambda_x)*e^{-Kd*z}$, and the upward attenuation coefficient is K_u, then with the consideration that D_d, D_u and the irradiance reflectance $R(\lambda_x)$ are depth independent, the sub-surface irradiance for a infinite water column due to the in-elastic scattering is

$$E_{uf}(0^-,\lambda)=2\pi(D_d+D_uR)\int_{\lambda_x}\frac{\beta_f(\lambda_x,\lambda)E_d(0^-,\lambda_x)}{K_u(\lambda)+K_d(\lambda_x)}d\lambda_x \tag{17}$$

Define Q_I as the Q factor for the in-elastic scattering field, then the subsurface radiance due to in-elastic scattering is

$$L_f(0^-,\lambda)=\frac{2\pi(1+2*R)}{Q_I}\int_{\lambda_x}\frac{\beta_f(\lambda_x,\lambda)E_d(0^-,\lambda_x)}{2\kappa(\lambda)+\kappa(\lambda_x)}d\lambda_x \tag{18}$$

and the in-elastic scattering coefficient $\Phi(\lambda_x,\lambda)$ (m^{-1}/nm) is defined as

$$\phi(\lambda_x,\lambda)=\int_{\Omega}\beta_f(\alpha,\lambda_x,\lambda)*d\omega \tag{19}$$

Since $\beta_f(\alpha,\lambda_x,\lambda)$ is considered isotropic, then

$$\phi(\lambda_x,\lambda)=\beta_f(\lambda_x,\lambda)*4\pi \tag{20}$$

According to the definition of remote sensing reflectance, with Eq.18 and Eq.20, we have

$$R_{rsf}(\lambda)=I*\epsilon\int_{\lambda_x}\frac{\phi(\lambda_x,\lambda)*E_d(0^+,\lambda_x)}{[2\kappa(\lambda)+\kappa(\lambda_x)]*E_d(0^+,\lambda)}d\lambda_x \tag{21}$$

in which $\epsilon=[1+2R(\lambda_x)]/2Q_I$.

Defining $\eta(\lambda_x)$ as the quantum efficiency for the emission line excited by λ_x, for CDOM molecules

$$\eta(\lambda_x)=\int_\lambda \frac{\lambda}{\lambda_x}\frac{\phi(\lambda,\lambda_x)}{a_g(\lambda_x)}d\lambda \tag{22}$$

But $\Phi(\lambda_x,\lambda)$ is characterized by a log-normal curve[19], so

$$\phi(\lambda_x,\lambda)=\frac{\eta(\lambda_x)*\lambda_x*a_g(\lambda_x)}{\lambda*A}*e^{-s*[\ln\frac{\lambda-\lambda_0}{\sigma}]^2} \tag{23}$$

in which

$$A=\int_\lambda e^{-s*[\ln\frac{\lambda-\lambda_0}{\sigma}]^2}d\lambda \tag{24}$$

where $\eta(\lambda_x)$, λ_0, s, A and σ are functions of the type of CDOM and λ_x.

In general, $b_b << a$ for most oceanic waters[16], so κ is close to a. For $R(\lambda_x)$ values of about .05, then $\epsilon \simeq 1.1/2Q_I$. And, based on the calculation for chl-a fluorescence made by Gordon[12], the Q factor for in-elastic scattering is ~3.7. Then combining Eq.21 and Eq.23, the remote sensing reflectance due to CDOM fluorescence can be reduced to

$$R_{rsF}(\lambda)=.1486I*F(\lambda) \tag{25}$$

$$F(\lambda)=\int_{\lambda_x}\eta(\lambda_x)\frac{\lambda_x}{\lambda}\frac{a_g(\lambda_x)*E_d(0^+,\lambda_x)}{[2a(\lambda)+a(\lambda_x)]*E_d(0^+,\lambda)}*\frac{e^{-s*[\ln\frac{\lambda-\lambda_0}{\sigma}]^2}}{A}d\lambda_x \tag{26}$$

Unlike broad-band (~100nm) CDOM fluorescence, the water Raman emission has a half-band width of about 20 nm[20]. Omitting this band width, i.e. assuming a narrow Raman emission, the in-elastic scattering coefficient $\Phi(\lambda_x,\lambda)$ can be related to Raman scattering coefficient as

$$\Phi(\lambda_x,\lambda)*d\lambda_x=b^R(\lambda_x)$$

and from Eq.21, with $\kappa \simeq a$, the remote sensing reflectance for water Raman is

$$R_{rsR}(\lambda)=.1486I*\frac{b^R(\lambda_x)*E_d(0^+,\lambda_x)}{[2a(\lambda)+a(\lambda_x)]*E_d(0^+,\lambda)} \tag{27}$$

and from the measurements of Marshall and Smith[21], $b^R(488)=2.6*10^{-4}$.

3. MODEL

For the modeling work, a_w and b_{bm} are already known[22], and a_p and a_g can be measured or modeled. What needs to be considered is how b_{bp}, Q, ρ, H, η, s, λ_0, and σ change with different environments.

R_{rsR}: Since this is a type of molecular scattering, $b^R(\lambda_x)$ is considered to have a wavelength dependence similar to that of water molecule scattering coefficient[23], i.e. a function of λ^{-4}. Thus $b^R(\lambda_x)=2.6*10^{-4}*(488/\lambda_x)^{-4}$. Then it is easy to calculate R_{rsR} using Eq. 27 when the total absorption is known. The transmittance of the air-sea interface for the solar irradiance is considered wavelength independent. The incoming light field was measured with a Licor-1800[24], which is used in our R_{rsR} and R_{rsf} calculations. The calculations of R_{rsR} and R_{rsf} are begun from the excitation wavelength 300nm. The frequency shift for water Raman scattering is fixed at 3512cm^{-1} as an average from Collins et al[20].

R_{rsf}: As can be seen from Eq.26, there are at least four variables $(\eta(\lambda_x),s,\lambda_0,\sigma)$ needed to calculate the remote sensing reflectance due to CDOM fluorescence when the total absorption is known. From lab measurements of CDOM fluorescence for our West Florida Shelf experiments, the quantum efficiency $\eta(\lambda_x)$ was between $\sim$0.5% and $\sim$1.5%, and generally is rather constant for different excitation wavelengths. The slope s was about 10, $\lambda_0 \sim (.95\lambda_x-45)$, $\sigma \sim (195-\lambda_x/5)$, all of which were quite constant for different stations (see Hawes et al[19], this volume.)

R_{rsb}: This value depends not only on the optical properties of the water body, but also on water depth and the bottom albedo. In the modeling work, the water depth comes from the Provisional Chart for Gulf Coast (C&GS #1003), and the bottom albedo was based on the measurements of bottom samples from 10m depth with values of 0.2 to 0.25 (used for Station 1) and from 20m depth with values from 0.4 to 0.5 (used for Stations 2 and 3). The semi-diffuse attenuation coefficient κ is assumed equal to total absorption $a(\lambda)$.

R_{rsw}: When using Eq.11 to model the measured R_{rsw}, a_w, b_{bm} and total absorption $a(\lambda)$ are already known, but evaluation of b_{bp} and Q for different water bodies and solar zenith angles is required. For a_p, a_g and b_{bp}, models exist for open ocean or "Case I" waters[5,25], but for other areas, a_p and a_g must be measured or modeled. The particulate backscattering coefficient b_{bp} has been considered to be a spectral function of λ^{-1} or a constant for near-shore waters[25,26].

For the factor Q, however, there are only a few measurements, and its values have been reported from 3.2 to 12[13]. Theoretically, not much attention has been paid to factors affecting Q, perhaps because generally $L_u(-,\lambda,\theta,\phi)$ is considered close to Lambertian due to multiple scattering. Q has been taken to be about 4.7 and spectrally constant from 440 to 550nm[27], although Kirk[28] gives Q as $\sim$4.9, and Gordon[29] suggests a value of $\sim$3.4. For many studies, Q is often arbitrarily chosen as a spectral constant[9,13,26]. From Davis' recent measurements (unpublished), however, as Carder et al.[6] mentioned recently, Q is not spectrally constant for the waters studied in this report. From these measurements, generally, there is a trend for Q to increase with wavelength. To model R_{rsw} for a region where b_{bp} does not covary with pigment concentration and a spectral Q factor needs to be considered, at least four parameters are needed.

Here we consider the water-leaving radiance of the water column L_{uw} as two parts, one from water molecules L_{um}, and one from particles L_{up}, with the assumption of no interference between these two. Then Eq.11 can be adjusted as

$$R_{rsw} = \frac{.33I}{a} * (\frac{b_{bm}}{Q_m} + \frac{b_{bp}}{Q_p}) * [1 - e^{-3 * D_d * a * H}] \quad (28)$$

in which Q_m and Q_p are the Q factors for water molecules and particles and, are defined as

$$Q_m = \frac{E_{um}(-,\lambda)}{L_{um}(-,\lambda)}, Q_p = \frac{E_{up}(-,\lambda)}{L_{up}(-,\lambda)} \quad (29)$$

We are aware of neither theoretical predictions, nor experimental measurements of Q_m. However, to first order an estimate can be made based upon the phase function and illumination geometry. For a given illumination geometry, the shape of the radiance distribution within the water is determined primarily by the volume scattering function through single scattering: e.g. Gordon[30] suggested a single-scattering approximation can be used to specify the variation of $R(\lambda)$ with the solar zenith angle, and Kirk[17] used single-scattering to describe the average cosine. Combining the approach used by Jerlov[31] to provide an estimation of radiance and irradiance with sun angle and depth, Austin's definition of Q factor[14], and the volume scattering function of water molecules given by Morel[32], the Q_m factor for sun light was calculated. The results can be approximated by the following simple function:

$$Q_m^{sun} = 5.92 - 3.05\cos(j) \quad (30)$$

With the assumption that the Q_m factor due to skylight is about 3.14, the effective Q_m for a mixture of sunlight and skylight is given by

$$Q_m = \frac{1+\gamma}{1+\gamma\frac{Q_m^{sun}}{3.14}} Q_m^{sun} \quad (31)$$

if we define $\gamma = E_d^{sky}/E_d^{sun}$, and calculate γ using Gregg and Carder's model[33]. Model results of Q_m^{sun} centered about 3.23 for environments studied in this contribution and are shown in Table 3.

Since we do not know the volume scattering function of the water sample, b_{bp} and Q_p can not be estimated using such a direct approach. However, since b_{bp} can be considered a function of $b_{bp}(400)*(400/\lambda)^n$ as in Smith and Baker[22], we may also consider Q_p to be a function of $Q_p(400)*(400/\lambda)^m$. Then b_{bp}/Q_p can be combined and modeled as $X*(400/\lambda)^Y$, where X and Y are two unknowns determined by specific particulate suites and solar illumination scenarios. After calculating R_{rsR}, R_{rsf} and R_{rsb}, only X and Y are left as unknowns. By matching the modeled R_{rsw} and the residual of R_{rs}-R_{rsR}-R_{rsf}-R_{rsb} at shorter (e.g. ~400nm) and longer (e.g. > 700 nm) wavelengths, X and Y were derived using a predictor-corrector approach as in Carder and Steward[13].

Using the methodology described above, two fields of R_{rs} are modeled: 1) Lake Tahoe with a clear, deep water column; and 2) shallow, gelbstoff-rich coastal waters of the West Florida Shelf. Figures 1-4 show the results of this approach, and Table 2 provides the latitude, longitude and time/date of our experiments. Also Figure 5 shows the locations of West Florida Shelf stations, Table 3 shows the model parameters j, Q_m^{sun}, X and Y, $a_g(400)$ and $a_p(440)$, and measured $a_p(440)$ for each station. Table 4 shows

the ratio of R_{rsw}, R_{rsR}, R_{rsf} and R_{rsb} to the measured R_{rs} at 440nm and 550nm.

Table 1 Symbols and Definitions

$E_u(-,\lambda)$	= sub-surface upwelling irradiance
$E_d(-,\lambda)$	= sub-surface downwelling irradiance
$E_d(+,\lambda)$	= above-surface downwelling irradiance
$L_u(+,\lambda)$	= above-surface leaving radiance
$L_{uw}(+,\lambda)$	= above-surface leaving radiance from water molecules
$L_{uf}(+,\lambda)$	= above-surface leaving radiance from CDOM fluorescence
$L_{ub}(+,\lambda)$	= above-surface leaving radiance from bottom reflectance
$L_{uR}(+,\lambda)$	= above-surface leaving radiance from water Raman
$L_u(-,\lambda)$	= sub-surface leaving radiance
ρ	= bottom reflectance
H	= water depth
Φ	= in-elastic scattering coefficient
j	= under surface solar zenith angle
K_d	= downwelling diffuse attenuation coefficient
K_u	= upwelling diffuse attenuation coefficient
k	= radiance attenuation coefficient for Lambertian source
κ	= semi-diffuse attenuation coefficient, $a+b_b$

Table 2

Station	Latitude	Longitude	Time/Date
Lake Tahoe	39°7' N	120°5' W	17.5/8-9-90
WFS St1	27°27' N	82°55' W	14.5/3-4-90
WFS St2	27°20' N	83°03' W	17.0/3-4-90
WFS St3	27°12' N	83°11' W	18.9/3-4-90

Note: Time is in GMT. WFS=West Florida Shelf

4. FIELD MEASUREMENTS

Upwelling radiance above the sea surface and downwelling sky radiance were directly measured using the Spectron spectral radiometer (model SE-590), following the method of Carder et al[24]. Downwelling irradiance above the sea surface was measured with the SE-590 by viewing a Spectralon diffuse-reflection, calibration panel. Remote-sensing reflectance values were determined by removing reflected skylight from the upwelling radiance values[13,24], and dividing by the downwelling irradiance values. The absorption coefficients for particles were obtained for surface waters following the method developed by Mitchell and Kiefer[34]. Gelbstoff absorption a_g was derived from surface-layer K_d values determined with a Biospherical Instruments MER-1048, using the expression $a_g = k_d*\cos(j) - a_w - a_p$.

Table 3

Station	j	Q_m^{sun}	X	Y	$a_g(400)$	$a_p(440)$	measured $a_p(440)$
Tahoe	32	3.25	.0011	4.0	.027	.018	.019
WFS St1	35	3.31	.0088	1.4	.170	.029	.053
WFS St2	26	3.15	.0019	2.4	.069	.040	.040
WFS St3	27	3.17	.0010	2.4	.065	.029	.030

TABLE 4

Station		Tahoe	WFS St1	WFS St2	WFS St3
R_{rsw}/R_{rs}^m	440nm	.933	.920	.896	.876
	550nm	.890	.902	.789	.817
R_{rsf}/R_{rs}^m	440nm	.018	.021	.029	.063
	550nm	.019	.008	.018	.038
R_{rsR}/R_{rs}^m	440nm	.035	.003	.022	.032
	550nm	.109	.005	.043	.077
R_{rsb}/R_{rs}^m	440nm		.012	.038	.015
	550nm		.089	.123	.033

Note: R_{rs}^m represents the measured remote sensing reflectance.

5.RESULTS AND DISCUSSION

For Lake Tahoe (Fig.1), the modeled R_{rs} curve fit the measured curve very well. From Table 4 we find that, water Raman had a bigger influence on the reflectance than did CDOM fluorescence due to less gelbstoff. At 550nm, the influence of water Raman was over 10%, close to the 15% value for sub-surface irradiance reflectance of Marshall and Smith[21] and 12% value of Stavn[35] for 490nm. This means caution must be exercised when using this wavelength band to measure water depth for clear water bodies.

For West Florida Shelf Station 1 (Fig. 2), the modeled R_{rs} curve suggests a high particulate concentration (b_{bp}) and large particulate sizes for this station, since X is big and Y is small. At the same time, the bottom reflectance was derived using a 13.7m water depth and a spectrally constant bottom albedo (0.20), and a CDOM fluorescence efficiency of $\eta = 1.0\%$. For this station, a_p used in the model is about 45% smaller than the measured a_p. Some difficulty in the measurement approach for a_p or chlorophyll specific absorption a_ϕ may have occurred, due perhaps to the effects of the pad correction of "beta factor"[36] and the package effect[37], especially for this inshore station. For the offshore stations, modeled a_p is within $\pm 5\%$ of the measured a_p. For West Florida Shelf Station 2 (Fig. 3), the measured R_{rs} is modeled using a 0.50 bottom reflectance with 25m water depth, and a CDOM fluorescence efficiency $\eta = 1.0\%$. For

West Florida Shelf Station 3 (Fig. 4), the measured R_{rs} is modeled using 0.50 bottom reflectance with 36m water depth, and a CDOM fluorescence efficiency $\eta = 1.5\%$.

For West Florida Shelf stations, the general model agreement with measurements is excellent, with small differences near 570nm, where the measured R_{rs} > modeled R_{rs}. There are three possible reasons for this: a) bottom albedo, b) phycoerythrin fluorescence[38], and c) water absorption coefficient. A spectrally constant bottom albedo was used in the model; gradual spectral increases occur in the albedo in this region, but they could not account for the sharp increase and then decrease required for the R_{rs} curves to converge. More realistic explanations include the lack of a term for phycoerythrin fluorescence, and the differences between the reported water absorption coefficients by Smith and Baker[22] and Tam and Patel[39]. Both explanations need more study.

Spitzer and Dirks[40] made theoretical predictions regarding the contributions on the sub-surface irradiance reflectance R(-) due to CDOM fluorescence. They used a Gaussian expression for emission with wavelength and a quantum efficiency $\eta = .0045$. Our model and measurement work[19] shows that the measured remote sensing reflectance can be explained in part by CDOM fluorescence, with the quantum efficiencies for the model curves twice to thrice the value .0045. It can be found from Table 4 that the combination of R_{rsR}, R_{rsf} and R_{rsb} can influence the ratio of $R_{rs}(440)/R_{rs}(550)$ by as much as 14%. This influence can cause a difference of $\sim 20\%$ relative to the pigment concentration determined by the power-law expression. $R_{rsw}(490)/R_{rs}^{m}(490)$ values as low as 0.77 were found, suggesting that for intermediate wavelengths great care must be taken when interpreting coastal remote sensing curves.

6. SUMMARY

Contributions to the water-leaving radiance signals in coastal waters of the West Florida Shelf were attributed by modeling activities to elastic scattering by water molecules, suspended particles and the bottom, and to in-elastic scattering by water Raman and CDOM or gelbstoff fluorescence. In-elastic scattering by pigments was not considered.

Close agreement was achieved between modeled and measured results for all stations when all of the above scattering mechanisms were included. As much as 23% of $R_{rs}(490)$ for a station in 25m of water was attributable to water Raman, CDOM fluorescence, and bottom reflectance. CDOM fluorescence contributed about 6.3% of the signal at 440nm for a station as far as 50km offshore. This work suggests that for many applications of remote sensing in coastal waters, serious errors can occur if CDOM fluorescence and bottom reflectance are ignored, even for stations 34 to 50km offshore in relatively deep (25 - 36m) waters.

7. ACKNOWLEDGEMENT

Financial support was provided by NASA through grant NAEW-465 and GSFC contract NAS5-30779, and by ONR through grant N00014-89-J-1091. Ship support was provided by the State of Florida through the Florida Institute of Oceanography. The authors wish to thank Bob Chen and Joan Hesler for administrative assistance, and Stacie Little for preparing the map.

8. References

1. Gordon, H.R., D.K. Clark, J.L. Mueller, and W.A. Hovis, 1980, "Phytoplankton pigments from the Nimbus-7 coastal Zone Color Scanner: Comparisons with surface measurements", Science, 210, 63-66.
2. Carder, K.L., R.G. Steward, J.H. Paul and G.A. Vargo, 1986, "Relationships between chlorophyll and ocean color constituents as they affect remote-sensing reflectance models," L&O, 31(2), 403-413.
3. Morel, A., 1988, "Optical modeling of the upper ocean in relation to its biogenous matter content (Case I Waters), JGR, 93(C9), 10,749-10,768.
4. Carder, K.L., W.W. Gregg, D.K. Costello, K. Haddad and J.M. Prospero, 1991, "Determination of Saharan dust radiance and chlorophyll from CZCS imagery," JGR, 96(D3), 5369-5378.
5. Morel, A. and J.M. Andre, 1991, "Pigment distribution and primary production in the western mediterranean as derived and modeled from Coastal Zone color Scanner observations", JGR, 96(C7), 12,685-12,698.
6. Carder, K.L., S.K. Hawes, K.A. Baker, R.C. Smith, R.G. Steward and B.G.Mitchell, 1991, "Reflectance model for quantifying chlorophyll a in the presence of productivity degradation products," JGR, 96(C11), 20599-20611.
7. Platt, T., C. Caverhill, and S. Sathyendranath, 1991, "Basin-scale estimates of oceanic primary production by remote sensing: the north atlantic", JGR, 96(C8), 15,147-15,159.
8. Walsh, J.J., 1988, On the nature of continental shelves, Academic Press.
9. Polcyn, F.C., W.L. Brown and I.J. Sattinger, 1970, "The measurement of water depth by remote sensing techniques", Report No. 8973-26-F, Infrared and Optics Lab., Willow Run Lab., Univ. Michigan. Ann Harbor.
10. Spitzer, D., and R.W.J. Dirks, 1987, "Bottom influence on the reflectance of the sea," Int. J. Remote Sensing, 8(3), 279-290.
11. Lyzenga, D.R., 1978, "Passive remote sensing techniques for mapping water depth and bottom features", Appl. Optics, 17(3), 379-383.
12. Gordon, H.R., 1979, "Diffuse reflectance of the ocean: the theory of its augmentation by chl-a fluorescence at 685nm", Appl. Optics, 18(8), 1161-1166.
13. Carder, K.L. and R.G. Steward, 1985, "A remote sensing reflectance model of a red tide dinoflagellate off West Florida," L&O, 30(2), 286-298.
14. Austin, R.W., 1974, "Inherent spectral radiance signatures of the ocean surface," Ocean color Analysis, SIO Ref. 7410, April.
15. Gordon, H.R., O.B. Brown and M.M. Jacobs, 1975, "Computed relationship between the inherent and apparent optical properties of a flat homogeneous ocean," Appl. Optics, 14, 417-427.
16. Morel, A. and L. Prieur, 1977, "Analysis of variations in ocean color," L&O, 22(4), 709-722.
17. Kirk, J.T.O., 1991, "Volume scattering function, average cosines, and the underwater light field", L&O, 36(3), 455-467.
18. Kirk, J.T.O., 1984, "Dependence of relationship between inherent and apparent optical properties of water on solar altitude," L&O, 29(2), 350-356.
19. Hawes, S.K., K.L. Carder, G.R. Harvey, 1992, "Quantum fluorescence efficiencies of marine humic and fulvic acids: effects on ocean color and fluorometric detection", Ocean Optics XI, in press.
20. Collins, D.J., J.A. Bell, Ray Zanoni, I.S. McDermid, J.B., "Recent progress in the measurement of temperature and salinity by optical scattering", SPIE, vol. 489, Ocean Optics VII, 247-269.
21. Marshall, B.R. and R.C. Smith, 1990, "Raman scattering and in-water ocean properties," Appl. Optics, 29(1), 71-84.
22. Smith, R. C. and K.S. Baker, 1981, "Optical properties of the clearest natural waters," Appl. Optics,

20(2), 177-184.
23. Stavn, Robert H. and Alan D. Weidemann, 1988, "Optical modeling of clear ocean light fields: Raman scattering effects", Applied Optics, 27(19), 4002-4011.
24. Carder, K.L., P. Reinersman, R.F. Chen, F. Muller-Karger, C.O. Davis, M. Hamilton, 1992, "AVIRIS calibration and application in coastal oceanic enviroments", G. Vane ed., Remote sensing of enviroments, special issue on imaging spectrometry, in press.
25. Gordon, H.R. and A. Morel, 1983, "Remote assessment of ocean color for interpretation of satellite visible imagery: A review. Springer.
26. Peacock, T.G., K.L. Carder, C.O. Davis and R.G. Steward, "Effects of fluorescence and water Raman scattering on models of remote sensing reflectance," SPIE vol. 1302, Ocean Optics X, 303-319.
27. Austin, R.W., 1979, "Coastal zone color scanner radiometry", SPIE, vol. 208, Ocean Optics VI, 170-177.
28. Kirk, J.T.O., 1986, Light and photosynthhesis in aquatic ecosystems, Cambridge University Press.
29. Gordon, H.R., 1986, "Ocean color remote sensing: Influence of the particle phase function and solar zenith angle," Eos Trans AGU, 14, 1055.
30. Gordon, H.R., 1989, "Dependence of the diffuse reflectance of natural waters on the sun angle", L&O, 34(8), 1484-1489.
31. Jerlov, N.G., 1976, Marine Optics, Elsevier Oceanogrphy Series, 14, Elsevier Scientific Publishing Company, Amsterdam-Oxford-New York.
32. Morel, A., 1974, "Optical properties of pure water and pure sea water," in Optical Aspects of Oceanography, ed. by N.G. Jerlov and E.S. Nielsen, 1-24, Academic, San Diego, CA.
33. Gregg, W.W. and K.L. Carder, 1990, "A simple spectral solar irradiance model for cloudless maritime atmospheres", L&O, 35(8), 1657-1675.
34. Mitchell, B.G. and D.A. Kiefer, 1988, "Chl-a specific absorption and fluorescence excitation spectra for light limited phytoplankton," DSR, 35(5), 635-663.
35. Stavn, R.H., 1990, "Raman scattering effects at the shorter visible wavelengths in clear ocean waters", SPIE vol. 1302, Ocean Optics X, 94-100.
36. Bricaud, A. and D. Stramski, 1990, "Spectral absorption coefficients of living phytoplankton and nonalgal biogenous matter: A comparison between the Peru upwelling area and the Sargasso Sea", L&O, 35(3), 562-582.
37. Morel, A. and A. Bricaud, 1981, "Theoretical results concerning light absorption in a discrete medium, and application to specific absorption of phytoplankton", DSR, 28A(11), 1375-1393.
38. Yentsch, Charles S. and Clarice M. Yentch, 1979, "fluorescence spectral signatures: the characterization of phytoplankton populations by the use of excitation and emission spectra", J. Marine Research, 37(3), 471-483.
39. Tam, A.C., and C.K.N. Patel, 1979, "Optical absorptions of light and heavy water by laser optoacoustic spectroscopy", Appl. Optics, 18(19), 3348-3358.
40. Spitzer D. and R.W.J. Dirks, 1985, "Contamination of the reflectance of natural waters by solar-induced fluorescence of dissolved organic matter", Appl. Optics, 24(4), 444-445.

Fig. 1: Measured vs. modelled R_{rs} for a station at Lake Tahoe.

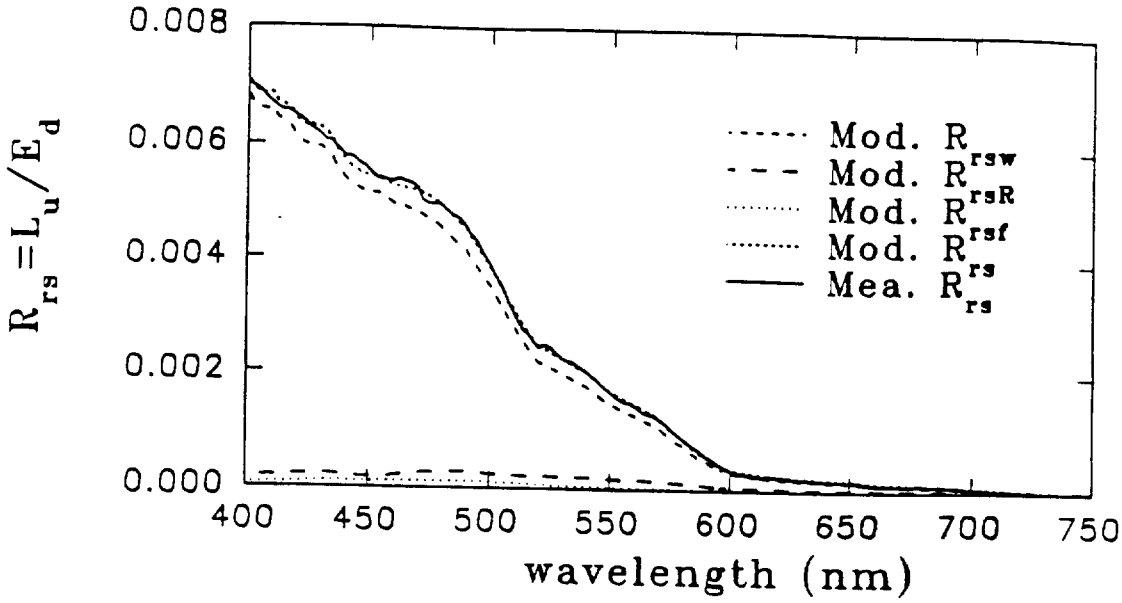

Fig. 2: Measured vs. modelled R_{rs} for station 1 of West Florida Shelf

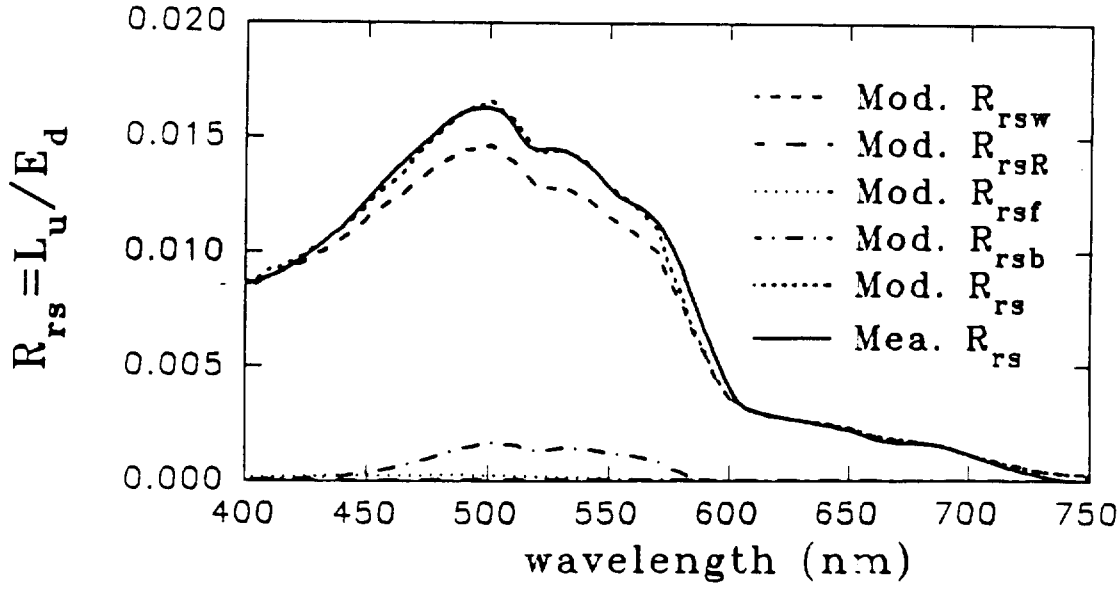

Fig. 3: Measured vs. modelled R_{rs} for station 2 of West Florida Shelf

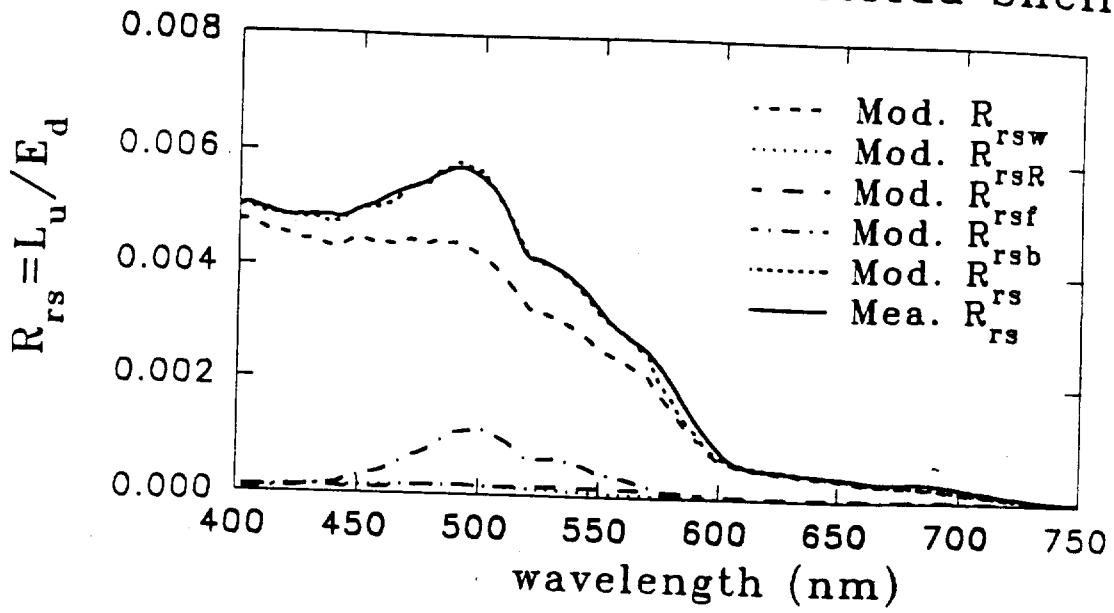

Fig. 4: Measured vs. modelled R_{rs} for station 3 of West Florida Shelf

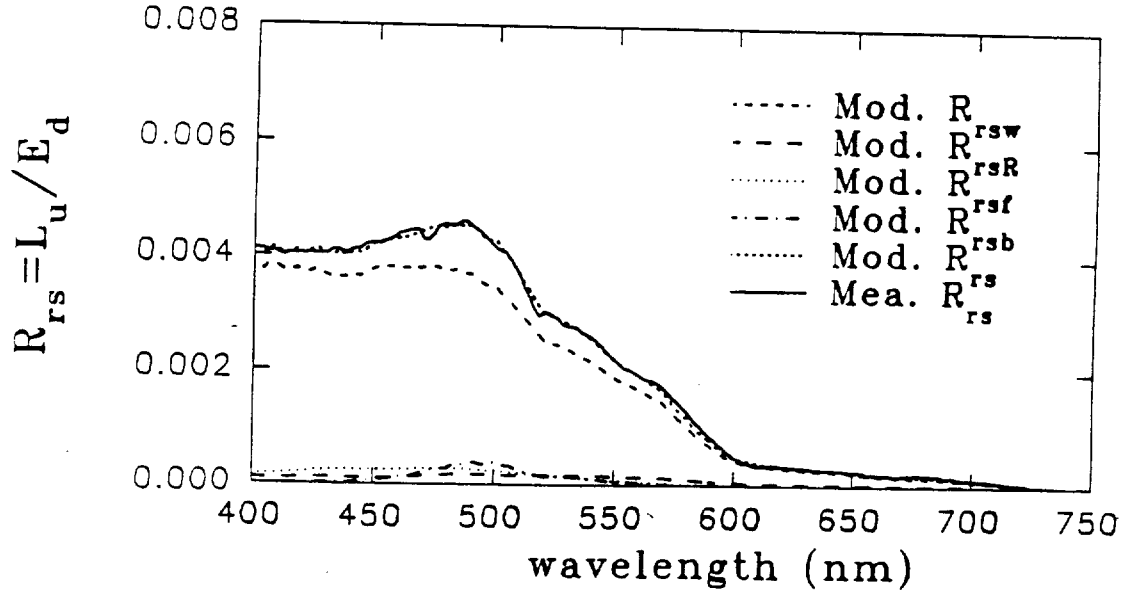

Fig. 5: Station locations of West Florida Shelf

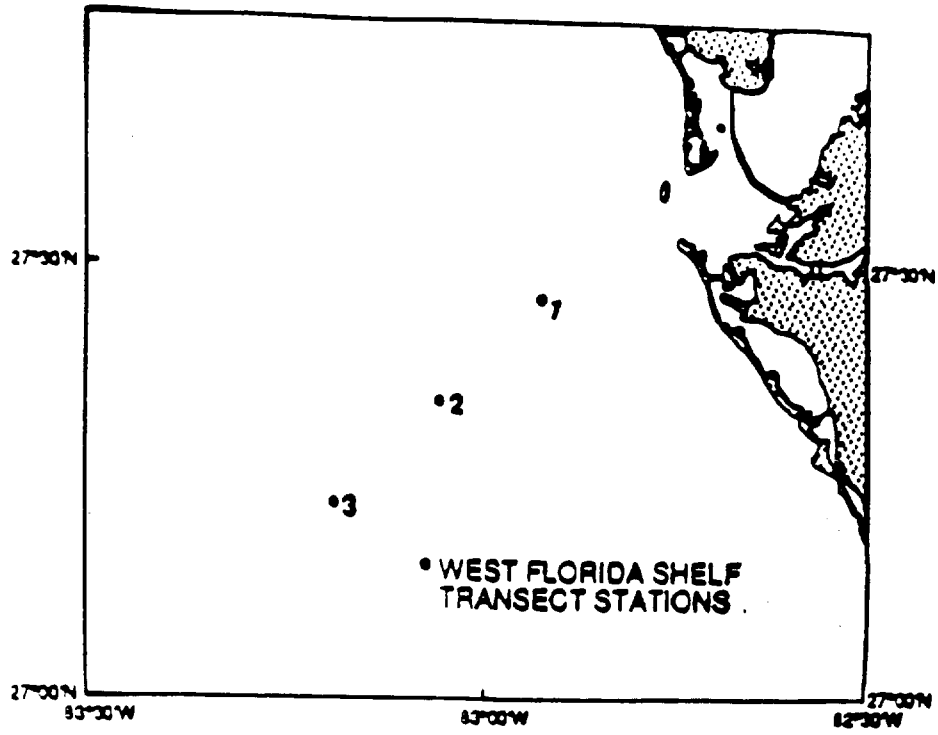

Fig. 6: Illumination geometry